DOE/PC/91155--T10

Coal-Fired High Performance Power Generating System

DE-AC22-92PC91155

[redacted] Quarterly Progress Report

for the Period October 1 – December 31, 1994

Prepared for

Pittsburgh Energy Technology Center
Pittsburgh, Pennsylvania

United Technologies Research Center
411 Silver Lane, East Hartford, Connecticut 06108

Coal-Fired High Performance Power Generating System

DE-AC22-92PC91155

Draft Quarterly Progress Report

for the Period October 1 – December 31, 1994

Prepared for

Pittsburgh Energy Technology Center
Pittsburgh, Pennsylvania

United Technologies Research Center
411 Silver Lane, East Hartford, Connecticut 06108

CONTENTS

TABLES

FIGURES

EXECUTIVE SUMMARY

This report covers work carried out under Task 3, Preliminary R and D, under contract DE-AC22-92PC91155, "Engineering Development of a Coal-Fired High Performance Power Generation System" between DOE Pittsburgh Energy Technology Center and United Technologies Research Center.

The goals of the program are to develop a coal-fired high performance power generation system (HIPPS) by the year 2000 that is capable of

- $>47\%$ thermal efficiency
- NO_x, SO_x and particulates $\leq 25\%$ NSPS
- cost $\geq 65\%$ of heat input
- all solid wastes benign

In our design consideration, we have tried to render all waste streams benign and if possible convert them to a commercial product. It appears that vitrified slag has commercial values. If the flyash is reinjected through the furnace, along with the dry bottom ash, then the amount of the less valuable solid waste stream (ash) can be minimized. A limitation on this procedure arises if it results in the buildup of toxic metal concentrations in either the slag, the flyash or other APCD components. We have assembled analytical tools to describe the progress of specific toxic metals in our system. The outline of the analytical procedure is presented in the first section of this report.

The strengths and corrosion resistance of five candidate refractories have been studied in this quarter. Some of the results are presented and compared for selected preparation conditions (mixing, drying time and drying temperatures).

A 100 hour pilot-scale slagging combustor test of the prototype radiant panel is being planned. Several potential refractory brick materials are under review and five will be selected for the first 100 hour test. The design of the prototype panel is presented along with some of the test requirements.

IMPACT OF FLY ASH RECYCLE ON TOXICITY OF SOLID HITAF RESIDUES

Background

One of the HIPPS program goals is to ensure that all solid waste streams are benign. The current HITAF design calls for a slagging combustion chamber to minimize deposit formation on the surface of the radiant heaters. The slag flow is removed by a slag tap at the base of the combustion chamber. The slagging combustion chamber is followed by water-wall sections of the furnace where soot-blowing will be utilized to remove dry deposits. Further downstream, particulate loading of the flue gas is minimized using an air pollution control device (APCD). The flyash removed in these sections become additional solid streams exiting the HIPPS process. The disposability of this ash, and thus its classification as 'benign', will vary depending on carbon content, toxic metal leachability, etc. Strict analyses of flyash materials are required before using these solid residues as recycled materials in roadbase, concrete filler, etc., or when disposing of the them in landfills.

Current practice with slagging or wet-bottom boilers is to reinject the flyash recovered in APCDs. The HITAF design will consider this possibility in order to minimize solid streams exiting the process. In principle, the flyash can be reinjected into the combustion chamber and combined with the slag stream to produce a vitrified product that can pass leachability tests. One concern, however, is that the recycle of flyash can result in a buildup of toxic metal concentrations over time in the HITAF system. Depending on the volatility of a particular metal and the overall ash composition, it can become preferentially enriched in either the slag or the flyash. A purge stream must be used to prevent excessive buildup, such that some fraction less than 100% of the flyash throughput should be recycled. Also, if the flyash purge stream is highly enriched in toxic metals, it may not qualify as a benign solid waste stream and it becomes questionable whether an optimal level of recycle can be determined.

To help quantify the effect of recycle on the processes of enrichment of slag and flyash, as well as potential increases for stack emissions, a simplified model of the slagging HITAF process was developed that incorporated the concept of flyash recycle. Variables were included to identify the effects of ash recycle ratio, particle entrainment, vaporization from slag and burning particles, and the efficiency of the air pollution control device (APCD) for particulate and fume control and the development will be presented in the following section.

Before proceeding with the model development, it should be noted that there is an additional benefit to flyash recycle as well; i.e., the possibility of reducing the emissions of toxic trace elements from the coal-fired HITAF through potential sorbent-like properties of the injected flyash. Although not currently one of the specific HIPPS goals, air toxic emissions are becoming a growing concern for coal-fired utilities. Several studies have indicated that there is a strong potential for the use of flyash-like materials for in-situ metal capture. Ratafia-Brown (1993) found reduced arsenic volatility when calcium carbonate was present in the ash; Helble et al. (1994) report that trace elements can be captured with ash materials for a gasification laboratory system. Eddings and Lighty (1994) found that

certain toxic metals such as Pb and Cd may react with alumino-silicate components in the soil at high temperatures rendering them nonleachable. Numerous studies have been performed by the University of Arizona, PSI Technology, US EPA and others which indicate the capture of volatile metals by certain solid sorbents.

Model Development

The slagging HITAF process is shown in Figure 1 with major input and output streams identified. The numbered nodes represent different points within the process where the mass of metal is either separated or combined. These points, described in Table 1, serve as nodes around which material balance expressions can be written. In addition, material balances can be written around the HITAF and APCD control volumes (shown by the gray boxes in Figure 1) and on the overall process. Also, a number of relations can be defined to allow variable adjustment of important parameters such as metal volatilities, recycle ratio, APCD efficiencies and entrainment rate. These parameters serve as process variables and are indicated in Figure 1 and are summarized in Table 2. It is important to understand the implementation of the different process variables as they are defined here. The APCD capture efficiency used in these calculations has two parts (two process variables – δ_1 and δ_2):

Table 1. Description of Node Points within Slagging HITAF Model

Node #	Description
1	Addition of recycled flyash to HITAF
2	Entrainment of burning coal and ash particles (β)
3	Vaporization of metal from slag (α_1)
4	Vaporization of metal from entrained coal and ash particles (α_2)
5	Combines vaporized metal from the two sources
6	APCD metal vapor/fume node – captures condensed metal fume at the efficiency specified (δ_2)
7	APCD particulate node – removes particulate at the efficiency specified (δ_1)
8	Combine escaping particulate and metal vapor/fume
9	Combine captured particulate and metal frame
10	Recycle node – specify the amount of the captured ash that is to be recycled back into the combustion chamber (γ)

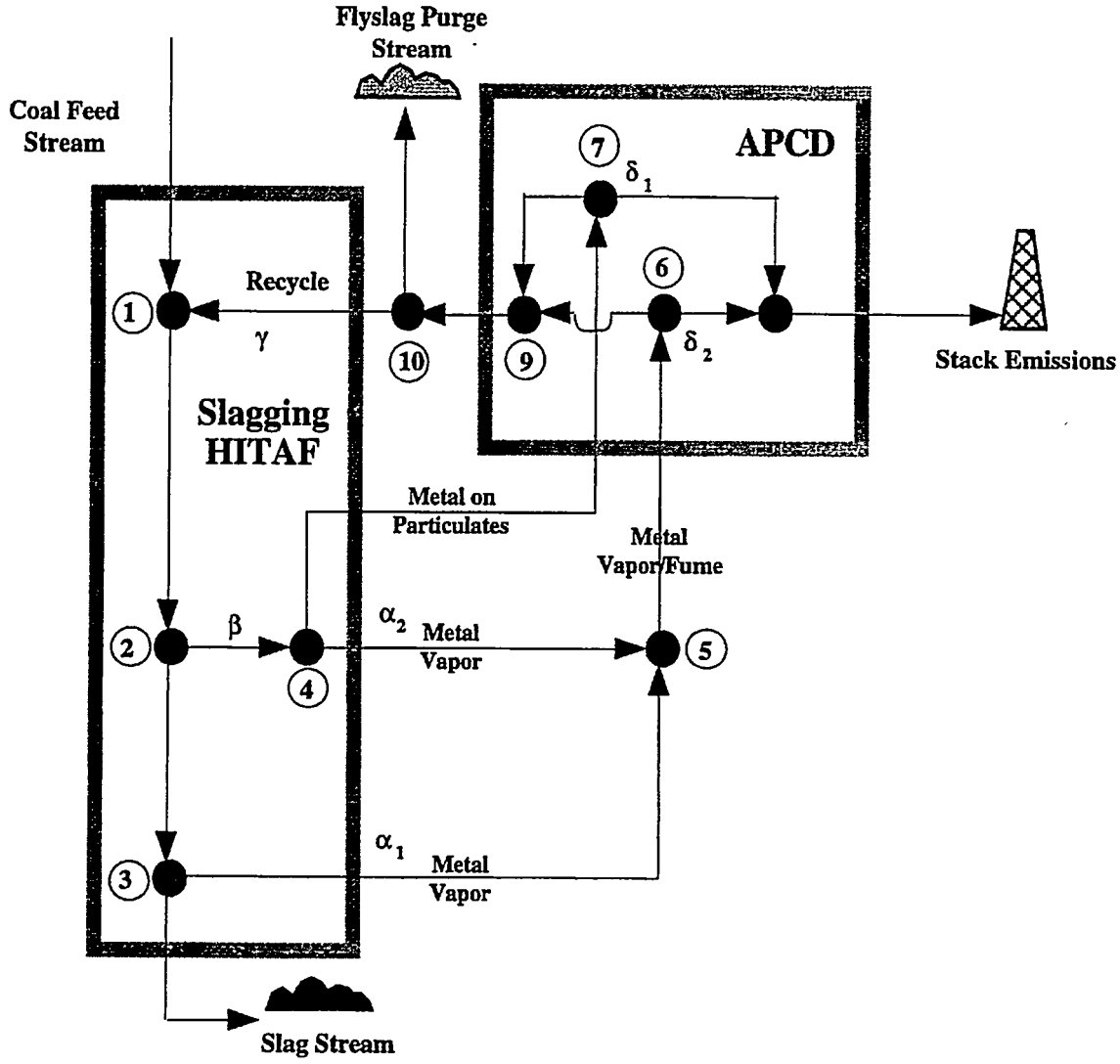

Figure 1. Process Diagram of Slagging Coal-Fired HITAF with Flyash Recycle.

Table 2. Definition of Process Variables

Symbol	Parameter Definition
α_1	Fraction of metal in slag that is vaporized
α_2	Fraction of metal in entrained particles that is vaporized
β	Fraction of ash that is entrained
δ_1	Efficiency of APCD for capturing particulate matter
δ_2	Efficiency of APCD for capturing vapor/fume/condensate
γ	Fraction of material captured in APCD that is recycled to the HITAF

- decrease or change in APCD particle collection efficiency due to malfunctioning or using different type of APCD (specified by variable δ_1)
- An increase in amount of metal on finer size fractions due to increased vaporization or homogeneous nucleation (resulting in fume formation) which will be more difficult to remove in the APCD (specified by a decrease in variable δ_2).

The metal vaporization or partitioning between condensed and gaseous phases also has two parts (the two process variables – α_1 and α_2):

- The amount of metal which vaporizes from the slag at the slag temperature and molten composition (α_1).
- The amount of metal which vaporizes from the entrained particles at their temperature.

The purpose for having two process variables for describing metal vaporization was to allow different mechanisms for describing metal volatility in the two potentially different environments (particularly if additives to the slag are used).

To fully resolve the material balance for the process model shown in Figure 1, seventeen different streams must be determined. If the coal feed mass flowrate of a given metal and the five process variables are specified, then only eight of the possible material balance expressions can be utilized to provide an independent solution. A solution was obtained using material balance expressions around nodes 2-8 and the HITAF material balance yielding the following expressions:

Slag stream mass flow rate:

$$\text{mass}_{\text{slag}} = \frac{m_1\,(1 - \alpha_1 - \beta + \alpha_1\beta)}{\Phi}$$

Where m_1 is the mass flowrate of the metal in the coal feed stream and Φ is defined by:

$$\Phi = 1 - \beta\delta_1\gamma + \alpha_2\beta\delta_1\gamma - \alpha_1\delta_2\gamma + \alpha_1\beta\delta_2\gamma - \alpha_2\beta\delta_2\gamma$$

Ash purge stream mass flow rate:

$$\text{mass}_{\text{purge}} = \frac{m_1\,(1 - \gamma)\,(\beta\delta_1 - \alpha_2\beta\delta_1 + \alpha_1\delta_2 - \alpha_1\beta\delta_2 + \alpha_2\beta\delta_2)}{\Phi}$$

Stack emission mass flow rate:

$$\text{mass}_{\text{slack}} = \frac{m_1 \left(\alpha_1 - \alpha_1\beta - \alpha_1\delta_2 + \alpha_1\beta\delta_2 - \alpha_2\beta\delta_2 + \beta - \beta\delta_1 + \alpha_2\beta\delta_1\right.}{\Phi}$$

This ash recycle model was applied to the slagging HITAF process using estimates of the different process variables to identify the sensitivity of the overall partitioning of toxic metals in a recycle system to each of these process variables. The initial calculations were carried out assuming a metal of intermediate volatility. For this case, it was assumed that half of the metal mass partitions from the slag into the gas phase ($\alpha_1 = 0.50$) and 75% of its mass will partition from burning or entrained particles ($\alpha_2 = 0.75$). The reasoning for this distribution was that the slag layer would be at a cooler temperature than the entrained/burning particles. The fraction of the flowing particulate that was removed as a slag layer was assumed to be 70%, thus the entrainment factor, β, was 0.30. Also, the particle collection efficiency for the APCD taken to be 0.999 (δ_1), or similar to an ordinary baghouse. The efficiency for collecting metal vapor, fume or condensate was a variable examined in the calculations, along with recycle ratio.

Results & Discussion

The results for stack emissions are plotted in Figure 2 as a percentage of the feed metal to the system, i.e., the metal introduced with the coal stream. As is shown, the amount of metal exiting the stack increases with increasing recycle ratio and with decreasing APCD efficiency for metal fume/vapor. The decrease in metal fume/vapor efficiency can be thought of as an increase in the amount of metal that condenses homogeneously to form submicron particulate. As more metal shifts to smaller size fractions, the efficiency for a given APCsD to capture that metal will decrease.

The partitioning between the different exits from the system is shown by the two cases in Figure 3. One case used a high capture efficiency ($\delta_2 = 0.99$) for the metal vapor/fume and the other used a low value ($\delta_2 = 0.50$). For the case of high efficiency ($\delta_2 = 0.99$), Figure 3 shows that the stack emissions are relatively small and that the slag-to-purge-stream partitioning is a strong function of recycle ratio. At high levels of recycle, most of the metal has partitioned to the slag, which is a favorable result. For the case of low efficiency ($\delta_2 = 0.50$), Figure 3 shows a much higher level of stack emissions and that the stack emissions are approaching the level contained in the slag. The comparison of the two cases in Figure 3 indicate that high levels of recycle are favorable for partitioning metals to the slag, thus rendering them environmentally benign; however, efforts must be expended to promote high capture efficiency of metal fume/vapor such as promoting particle agglomeration.

Although the overall metal mass exiting the system through the ash purge stream decreases with increasing recycle ratio (see Figure 3), the concentration of metal in the ash purge stream increases with increasing recycle ratio (see Figure 4). At low APCD fume efficiencies, however, the increase in

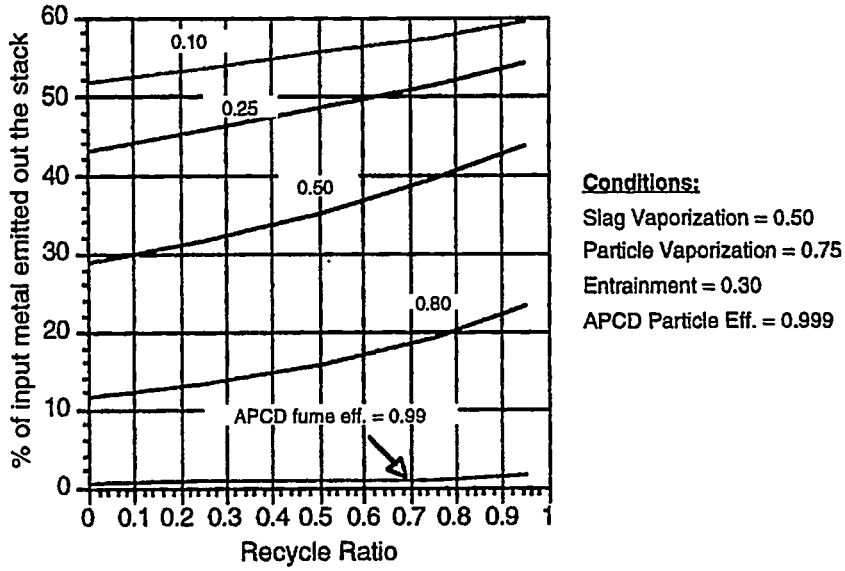

Figure 2. Effect of Recycle Ratio and Fume Efficiency on Stack Emissions.

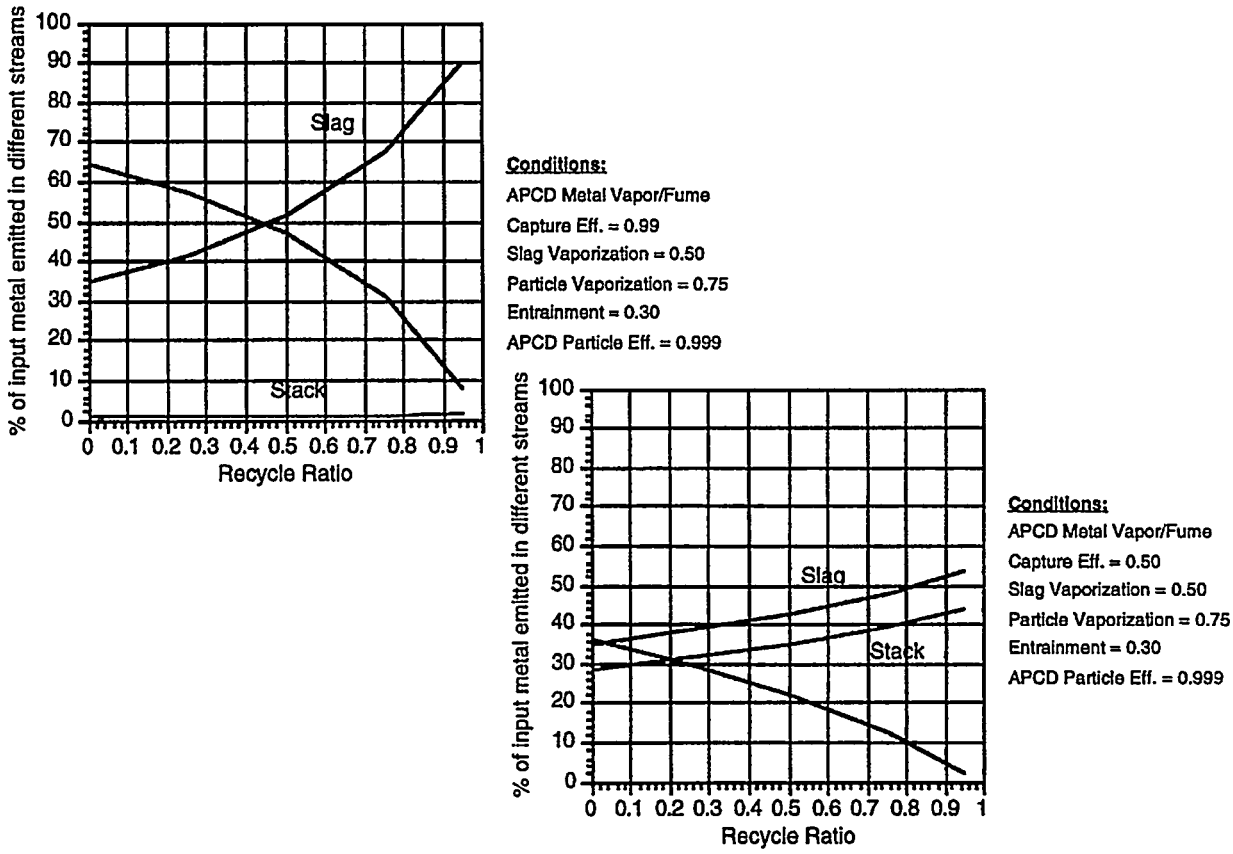

Figure 3. Effect of Recycle Ratio on Partitioning of Metal Between Different Exit Streams of the HITAF.

purge stream metal concentration with recycle is very minimal and actually decreases somewhat at very low efficiencies.

Slag concentration, shown in Figure 5, behaves similarly to the purge stream with increasing concentrations with increasing recycle at high fume efficiencies and slightly decreasing concentration at low fume efficiencies. Note that, although the concentrations are much lower than they are in the purge stream, they are not orders of magnitude lower. Stated differently, the purge concentration does become enriched in metal concentration with increasing recycle, but it does not become orders of magnitude more enriched than the slag stream concentration.

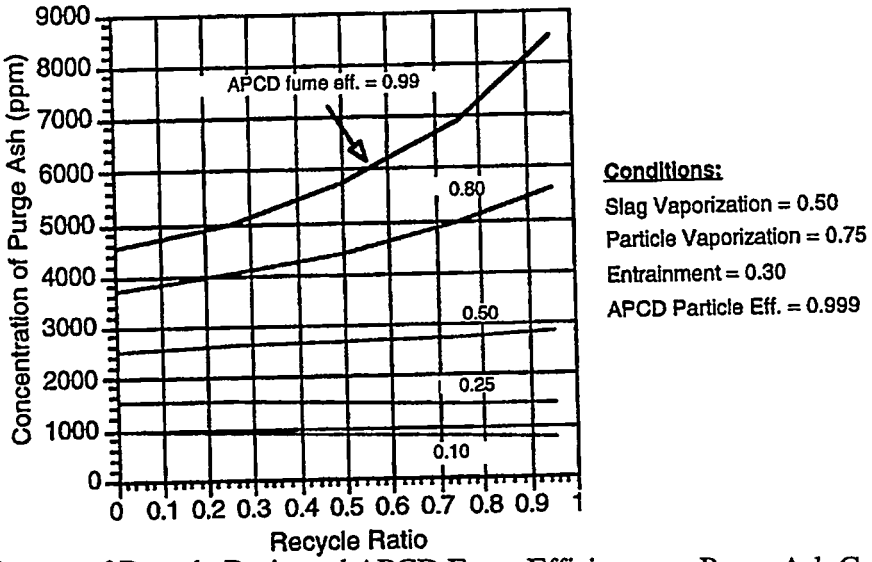

Figure 4. Impact of Recycle Ratio and APCD Fume Efficiency on Purge Ash Concentration.

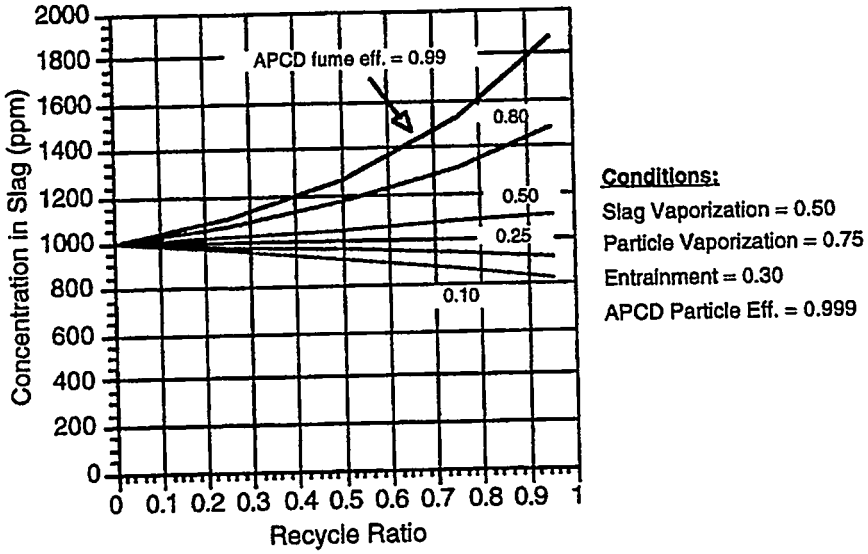

Figure 5. Impact of Recycle Ratio and APCD Fume Efficiency on Slag Concentration.

The partitioning between slag and purge streams can also be viewed as a ratio of masses as shown in Figure 6. As shown, there is a significant change in slag/purge mass ratio in the recycle ratio range of 0.75-0.95, indicating operation with high recycle ratios will provide the most partitioning to the slag stream. Note that the slag/purge mass ratio increases with decreasing APCD fume efficiency, which is likely the result of more metal exiting the stack. The calculations also indicated that although the slag/purge mass ratio varied with recycle ratio, the slag/purge concentration ratio was constant with recycle. The concentration ratio did vary somewhat with APCD fume efficiency.

Although not discussed here, the entrainment parameter, β, can be used to investigate effects due to different types of burners or different furnace designs (ones that have a greater tendency to throw particles to the walls). It should also be noted that this model formulation does not have an intrinsic mechanism for the effect that if recycle increases, the APCD fume efficiency for a semi-volatile metal can possibly decrease. This must be done artificially by changing the process variables. How important this is or how much it should change is not clear. The percentage of the feed in the purge stream varies w/APCD efficiency only by small amounts at high recycle ratios, but the percent of the feed in the stack varies significantly w/APCD fume efficiency at high recycle ratio.

The model was also applied to metal of high and low volatilities to illustrate the effect of recycle on other types of metal emissions. The conditions for these comparisons were an entrainment factor of $\beta = 0.30$, an APCD particulate efficiency of $\delta_1 = 0.999$ and an APCD fume efficiency of $\delta_2 = 0.50$. The metal vaporization parameters chosen were as follows: for the volatile metal – slag vaporization (α_1) = 0.90 and particle vaporization (α_2) = 0.99; for the medium-volatile metal – slag vaporization (α_1) = 0.50 and particle vaporization (α_2) = 0.75; for the low-volatile metal – slag vaporization (α1) = 0.10 and particle vaporization (α_2) = 0.20. The results for stack emissions and ash purge stream

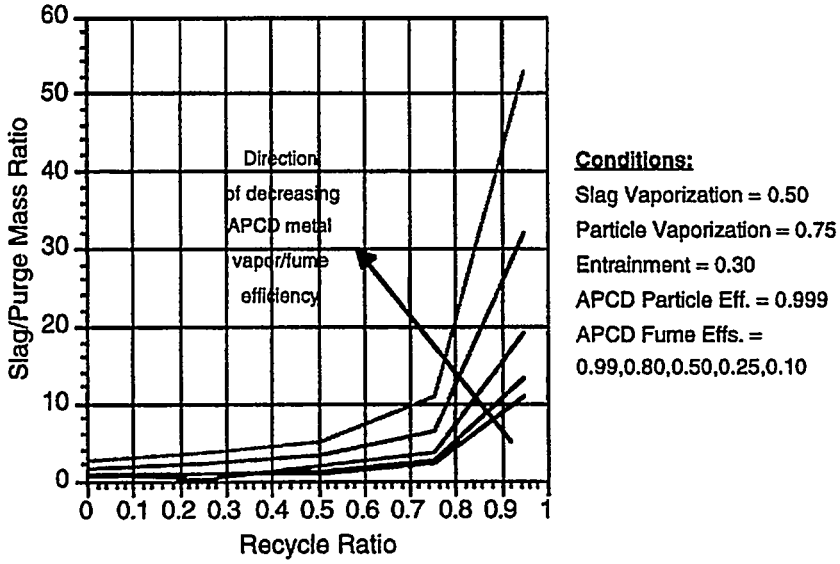

Figure 6. Effect of Recycle Ratio and SPCD Fume Efficiency on Slag/Purge Mass Ratio.

emissions are shown in Figure 7. As shown, purge stream emissions are very low for all volatilities at high recycle ratios but differ at low recycle ratios. The stack emissions vary considerably however at all levels of recycle with expected trends of high stack emissions for high volatility metals, intermediate levels of emissions for medium volatility metals, and low levels of stack emissions for low volatility metals.

Conclusions

The recycle of flyash in the HITAF has the potential to minimize one of the solid effluent streams from the HIPPS process. Depending on the implementation of the recycle process, the limited amount of flyash that is purged from the system may be usable as a recycled material. A model was developed and presented which described the impact of recycle rate and other operating conditions on metal partitioning between the slag stream the flyash purge stream and the stack. With the appropriate information on metal volatilities and APCD efficiencies, the recycle model presented can be a useful tool for analyzing a variety of HITAF operating conditions and can help define optimum conditions for using flyash recycle.

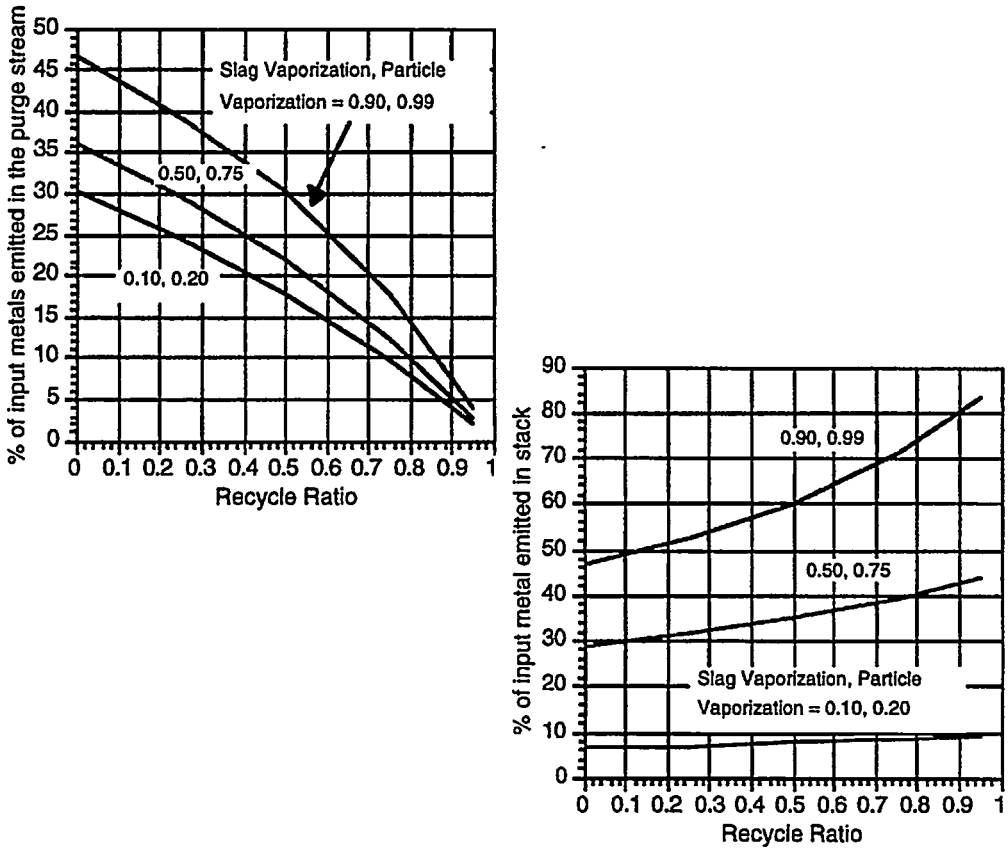

Figure 7. Effect of Recycle Ratio on Emissions of Metals of Different Volatilities.

PROCESSING OF BY-PRODUCT AND WASTE MATERIALS

Power Plant Location

The vicinity of Kenosha, Wisconsin, is the assumed site of a HiPPS plant to be used for economic evaluation of probable power plant by-product materials. It is located approximately 60 miles south of Milwaukee on the shores of Lake Michigan. The location is very significant in that it is near major U.S. cities that consume significant amounts of coal combustion by-products. Another significant factor is the availability of water transportation to other major metropolitan areas.

An important aspect of assessing marketability of by-products will be the use of integrative technological data manipulation software known as the Atlas Geographic Information Systems (GIS©). GIS is a software technology that permits the input, manipulation, analysis, and display of geographically referenced data. GIS contains a set of tools to perform a variety of functions directed towards integrating both map information and associated data. This capability will provide an effective means of indicating market areas in terms of such factors as travel distances, methods of transportation, available industries utilizing coal by-products, and competing materials similar to coal by-products.

The more precise a reference point available to GIS, the more beneficial its geographical application will be. For this reason, the community of Bain, Wisconsin was picked as the precise location of the coal combustion facility. The location of Bain is 1-2 miles southwest of Kenosha. An important reason for choosing Bain was its proximity to major railroad lines, a common method of transporting coal by-products for utilization.

Coal and Coal By-Products

Although a coal source has not officially been chosen, the leading candidate would be the Illinois No. 6 coal seam. When assessments are made on the expected chemical, mineralogical, and physical aspects of the by-products, the anticipated results will be based on this assumption.

The combustion by-products are assumed to be approximately 80% slag, 10% very fine fly ash, and 10% flue gas desulfurization sludge (FGD). Slag is a coal by-product that is used extensively in many parts of the United States. The potential utilization of the slag by-product has been initially identified in such applications as asphaltic concrete, skid-resistance material, roofing shingles, blasting grit, concrete masonry, and cement production. Interviews with prospective users will qualify the level of usage in these applications and lead to other sources of users and applications.

Fly ash is the most commonly used coal by-product, generally as a partial replacement for cement in concrete. The fly ash assumed to be produced for the proposed UTRC HiPPS system is considered to be an extremely fine particle size in comparison to conventional pulverized coal ash. This quality is important because specific surface area is a factor in assessing the use of coal fly ash in concrete applications.

Alternative FGD processes are designed to make by-products to use as fertilizers, agricultural lime substitutes, and high-purity gypsum for wallboard manufacturing. Potential utilization of all three by-products are being assessed. However, because slag constitutes the most significant quantity of the waste streams, a marketing emphasis is being placed on that particular material.

Market Study

Overcoming technological barriers, such as laboratory testing and field demonstrations, is but an initial step in power plant by-product utilization. The greatest challenges for marketing power plant by-products include convincing potential users that power plant by-products are beneficial raw materials and not inferior and hazardous waste products and convincing regulatory agencies to develop requirements that will clarify and promote reuse options.

Coal combustion wastes are exempted from federal hazardous waste regulations (subtitle C) under the Resource Conservation and Recovery Act (RCRA). As a result of this exemption, coal ash may be regulated under state solid waste requirements in accordance with RCRA Subtitle D. However, with no guidance on the reuse of coal ash provided by the U.S. Environmental Protection Agency (EPA) state regulations vary significantly. Individual state regulations can be vague and/or extremely conservative resulting in a complicated approval process. Thus it is important to be aware of and understand each state's regulations prior to pursuing an ash-marketing program.

In an unpublished report by the American Coal Ash Association, a nationwide survey was performed in an effort to identify regulatory barriers to the beneficial use of power plant by-products and to identify areas where regulatory reform may be warranted. The results of the survey summarize the solid waste regulations and/or policies pertaining to power plant by-product utilization on a state-by-state basis.

In Wisconsin, coal ash is exempt from the hazardous waste regulation and is regulated as special waste under solid waste regulations. Provisions allow coal ash to be exempted from the state landfill requirement if beneficially used. The ash is still considered a waste and the exemption must be requested and approved under a provision for the beneficial use of utility ash. Bottom ash (or slag) can be used as a fill material for road subbase, for foundations of a building, and under parking lots.

As in Wisconsin, the state of Illinois exempts coal ash from the hazardous waste regulations. It is regulated as a special solid waste under state regulations. No specific regulations address utilization, and requests are handled on a case-by-case basis.

The determination of net revenues from the sale of by-products will involve 1) estimating the initial required capital outlay, if any, needed to prepare and/or market by-products to the appropriate users, 2) estimating the operating costs per unit of by-product sold based on inputs of labor, transportation, and related costs, and 3) estimating the potential market for by-products in the relevant marketing area, including an identification of potential users, prices, and annual incremental

revenues. In addition to determining the commercial value of plant by-product streams, the cost savings in reduced storage of the by-products must also be determined.

Preliminary studies have indicated a potential need for initial capital outlay. It may be necessary to establish extra storage capabilities and facilities, including transport systems (pneumatic, water sluicing, etc.) to and from collection points and systems. Besides internal transportation, rail line service must be established for economical transport out of the power plant area. The objective of any ash utilization program will stress keeping in line with the minimum conversion efficiency goal of 47%.

Estimating operating costs per unit of by-product sold ($ per ton) will be performed based on requirements of labor, transportation, and related costs to achieve the necessary level of quality assurance. A consistent product is crucial to maintaining a client base for a continuous coal ash utilization program, and this requirement may warrant establishing a role for a by-product quality assurance manager.

PROPERTIES OF ASH DEPOSITS

Refractory Experiments

Strength testing of three commercially available and two experimental monolithic refractories was initiated. The commercial materials were obtained from Plibrico and included two alumina-based and one silicon carbide-based formulations. The alumina-based materials were designated (L-2825), containing 99.6% Al_2O_3 and 0.05% SiO_2, and Plicast Cement Free 96 (L-2803), containing 95.3% Al_2O_3 and 3.8% SiO_2. The SiC-based mix (L-2824) was composed of 88.2% SiC, 4.9% Al_2O_3, and 6.6% SiO_2. The experimental refractories were prepared at the EERC and consist of SiC aggregate with an alumina binder. They were prepared in aggregate-to-binder ratios of 70:30 and 90:10. For each of the refractories, two corrosion blocks, and 3-5 room-temperature and 3-5 high-temperature strength blocks were prepared.

All of the materials were mixed in a Hobart Model N-50, 5-quart-capacity mixer. Water was added to each until a desired consistency was obtained. These samples were vibrated by placing the molds on top of a Spex Shatterbox for the required amount of time. Drying was done in three stages. First, the blocks were cured at room temperature (25°C), then they were heated in a Boekel low-temperature drying oven for 8 hours at 80°C, after which the temperature was raised to 110°C overnight. The final firing was done for the high-temperature blocks and the corrosion blocks using a Keith Model No. KKSK 999 3100 high-temperature furnace. A program sequence was set up to slowly ramp to 1500°C, hold for 12 hours, then slowly cool down to room temperature. Table 7 gives information regarding each of the Plibrico refractories.

These three materials were all relatively easy to work with, except for a few areas affecting the processes. Bubbles formed in the L-2825 but were removed during the vibrating sequence using a sharp instrument. After 5 min of mixing, the L-2803 material formed small pebble-like agglomerates, and an additional 3 min of mixing was needed to make it workable. The longer this particular material was mixed, the wetter it became. The texture of L-2824 was sandlike, and the consistency did not change after extended mixing or vibrating, so vibrating was eliminated.

Tables 3 and 4 give preparation information about the commercially available and experimental refractories, respectively.

Table 3. Commercially Available Monolithic Refractories

Mix	% H_2O	Time Vibrated, min	Drying Time, hr	Drying Temp., °C	Firing Temp., °C
L-2825	7.4	5	24 8 16	25 80 110	1500
L-2803	5.2	8	24 8 16	25 80 110	1500
L-2824	6.0	none	24 8 16	25 80 110	1500

Table 4. Experimental Refractories

Mix	% H_2O	Time Vibrated, min	Drying Time, hr	Drying Temp., °C	Firing Temp., °C
90:10	9.5	5	24 8 16	25 80 110	1500
70:30	17.5*	5	24 8 16	25 80 110	1500
* Plasticizer added					

The mixing sequence was altered for the two experimental refractories. The dry ingredients were mixed for 2 min prior to adding the water. The drying was the same as previous samples. After drying, a layer approximately 1/4 in. thick on top of most of the 70:30 blocks fractured and was easily removed. X-ray diffraction and x-ray fluorescence analyses were done on one sample to determine the composition. The data showed it to be fine particles of binder and SiC. The sample may have been vibrated too long causing the particles to rise to the top and to form a weak zone that fractured when heated. Further experimentation is required to stabilize the mixture while drying.

The as-dried compressive strengths of the refractories were determined at room temperature using a Forney QC-400C-D2 compression testing machine. The following information has been included in Figure 8. The Plicast cement-free alumina refractory (L-2803) had the greatest average compressive strength at 33,500 psi (five samples). The 99.6% alumina mix (L-2825) was next highest with 17,500 psi (three samples). The third highest was the experimental 70:30 SiC:alumina mixture with approximately 15,000 psi (four samples). These samples varied greatly in strength from 19,000 to 11,000 psi. This inconsistency could be partly due to operator error, and the problems encountered with this particular mixture. The fourth highest was the SiC-based L-2824 which averaged 6900 psi (three samples). The 90:10 SiC:alumina mix was the weakest at 6400 psi (four samples). Much like the 70:30 samples, the results were somewhat inconsistent. The first two samples yielded about 7300 psi

while the last two were around 5400 psi. A slight variation in the technique used to create the blocks, or in the operation of the Forney, could explain the inconsistency. This strength would still be sufficient to hold the refractory in place during firing in a UTRC HITAF scenario.

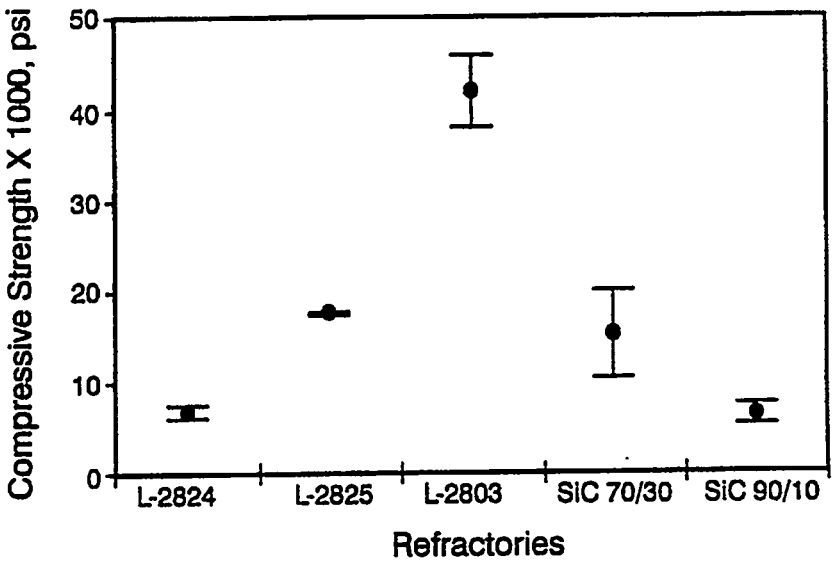

Figure 8. Room-Temperature Strength-Testing Results.

An Instron Model 8562 testing system was used to perform high-temperature strength testing. These tests are not completed at this time, but from the data available, the SiC-based mix (L-2824) has the greatest compressive strength at 1425°C. After firing the 70:30 SiC:alumina blocks, hairline cracks appeared throughout the blocks. The base of each block turned white from reacting with the alumina in the furnace. The high-temperature blocks were deformed. Expansion cracks radiated outward from the base of each block causing it to become fan-shaped. Until the separation problems are solved, strength testing of fired blocks will not be performed.

Corrosion testing using a high-calcium Illinois No. 6 slag received from Central Illinois Public Service Coffeen Plant has been completed. We are using slag collected from cyclone-fired boilers for the corrosion tests rather than laboratory-produced slag because it is created under conditions more like those of the UTRC HITAF than can be created in the laboratory. This slag was collected and characterized by the EERC for use by researchers studying slag corrosion of ceramics under funding by the U.S. Department of Energy (DOE) Advanced Research and Technology Development (AR&TD) Materials Program administered through Oak Ridge National Laboratory. The Illinois No. 6 coal used at the Coffeen plant is from a low-sulfur spur of the main seam. It has lower sulfur because it contains less pyrite (FeS_2) and hence less iron than more common Illinois No. 6 coals. The low iron level causes the viscosity of the slag to be very high, so the plant adds 1.5% limestone to the

coal to reduce it. The result is a high-calcium Illinois No. 6 slag with a viscosity-versus-temperature profile very similar to a more typical Illinois No. 6 slag. By comparing the corrosion rates of this slag with those of Powder River Basin and more normal Illinois No. 6 slags (also being collected under the AR&TD program), the relative importance of calcium content and slag viscosity in refractory corrosion can be delineated. This information will be necessary in predicting the effects of slag-flow additives on the corrosion rates of the refractory.

The static slag corrosion test was run at 1430° C. The refractory blocks were of the same design as blocks used in previous testing, but approximately twice as much slag was used to ensure that a surplus was available for reaction with the blocks. The test was terminated at 95 hr rather than 100 hr because of a technical problem with the furnace. The block was sliced in half vertically, and the refractory surface recession and slag penetrations were measured at three places on each half of each of the two blocks, for a total of twelve measurements per refractory type.

The following results from the corrosion test are included in Figure 9. Only a trace of slag remained in the alumina-based refractory slag wells. The slag was lost through penetration into the refractory for each of those samples. The blocks also had the greatest average slag penetration and appeared to corrode easily. The amount of penetration into the alumina refractories was surprising but may be due to the high calcium content of the slag, leading to the creation of calcium aluminate which dissolves in the slag. Slag penetration into the commercially available SiC-based refractory was also substantial, although about a 4-mm-thick layer of slag remained. No slag penetration was observed for the experimental refractories leaving a of slag 4-5 mm thick. The samples will be analyzed by SEM in the next quarter to determine the mechanisms of corrosion.

Although much more slag penetrated into the commercial than into the experimental refractories, Figure 10 shows that surface recession amounts were comparable. The 70:30 had the most recession, and it appears to be lower in density than the other refractories, probably because of the high amounts of water needed to make it workable. The lower density most likely led to the greater surface recession. Neither the 90:10 nor L-2824 had much surface recession, although a great deal of slag penetrated into the L-2824 (Figure 10). In the case of flowing slag where the slag is replenished and erosion is also a factor in surface recession, the commercial refractories would probably exhibit much more recession than the experimental refractories.

Dilatometric Analysis

Dilatometric analysis consists of measuring variations of the length of specimens caused by temperature or phase changes. It is employed for the determination of thermal expansion coefficients, changes in crystallographic parameters, and glass transition points. With no phase transformations, the length of specimen varies smoothly with temperature; if a phase transformation occurs in the material, the length (or volume) changes stepwise.

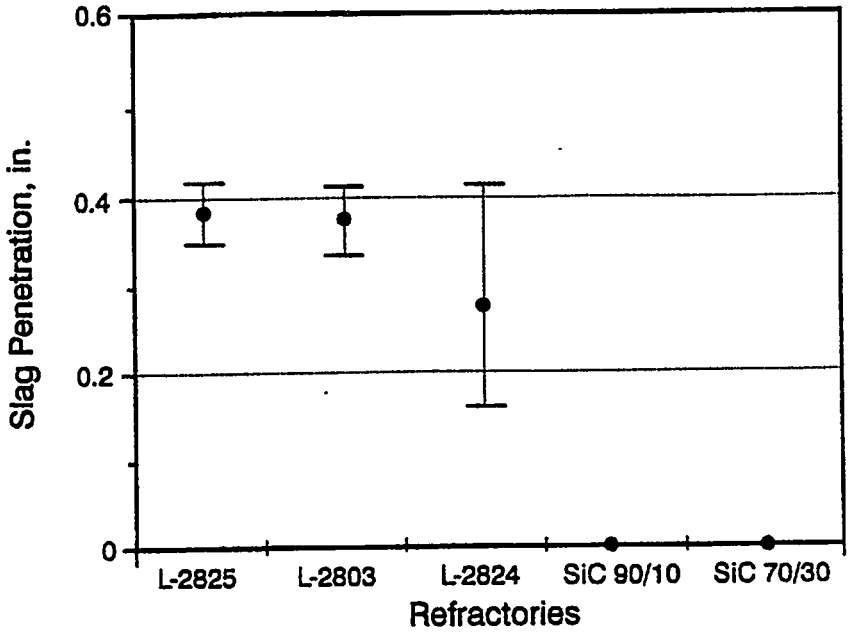

Figure 9. High-Calcium Illinois No. 6 Slag Penetration into the Refractories.

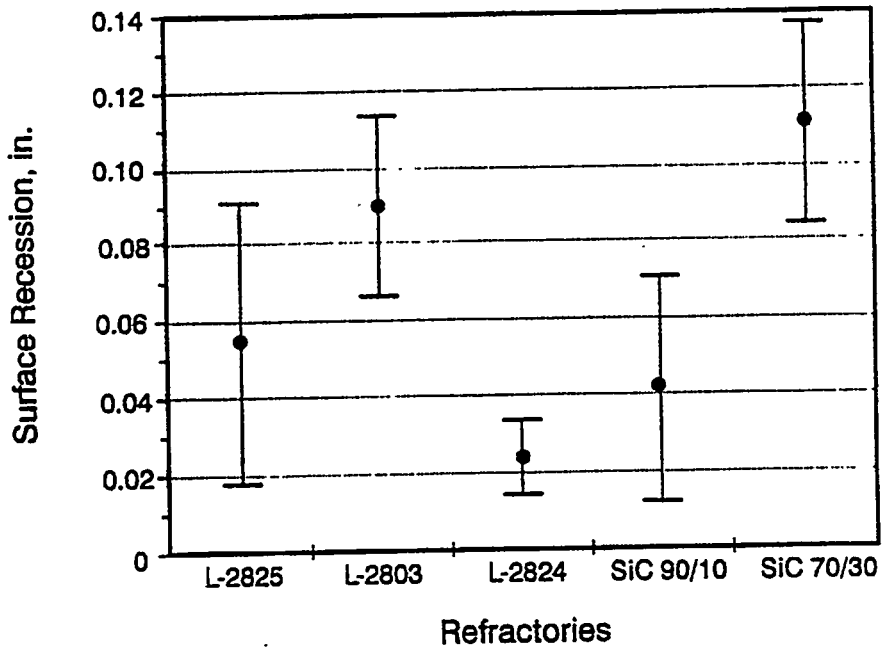

Figure 10. Refractory Surface Recession Due to Corrosion by High-Calcium Illinois No. 6 Slag.

Knowledge of the changes in size of materials versus temperature is necessary for proper engineering design of subsystems, but it is especially critical when the designs call for two dissimilar materials to be in contact. In the UTRC HITAF the high-temperature heat exchanger panel is such a subsystem. Composed of a high-temperature alloy covered by a corrosion resistant refractory, the materials must be chosen so that the refractory will not spall from the surface of the panel. Dilatometry can also be used to determine the rates of powder sintering, a capability we can use to measure temperature-dependent ash sintering rates so that we can determine the maximum length of time between ash removal cycles used for the convective pass air heater.

During this quarter, an Orton dilatometer model 1600D purchased from The Edward Orton, Jr., Ceramic Foundation was installed. The unit is designed to measure the linear expansion (or contraction) of specimens from room temperature to 1600°C. Data can be sent to a personal computer using the computer interface software for an IBM-compatible computer for storage and more detailed analysis.

Strength Testing of Materials

Design of a fully articulating, high-temperature, four-point flexure fixture has been completed, and bids are being accepted for its manufacture. The fixture will be used to determine the relative high-temperature strengths of new alloys and refractories. A sketch of the fixture is shown in Figure 11. It is to be constructed of both Norton NC-203, a hot-pressed alumina-bonded SiC, and Carborundum Hexoloy SA SiC, which will allow testing to be performed at temperatures up to 1500°C in air. The fixture has been designed to be used with SiC pushrods in the environmental test chamber of our Instron 8562 universal tester. The fixture will allow testing of both ASTM sizes "B" and "C," test bars 3 x 4 x 45 mm and 6 x 8 x 90 mm in size, respectively.

The fixture was designed for full articulation to adhere to the ASTM C1211-92 specifications for the possibility of twisted or uneven test specimen surfaces. This situation was thought likely to arise in the flexure testing of corroded samples or joined materials. Since no previous work with a high-temperature, fully articulating fixture of this kind has been found in the literature, assessment of the fixture is in order, and procedures will have to be developed to ensure sample alignment and positioning in the fixture before it is used routinely.

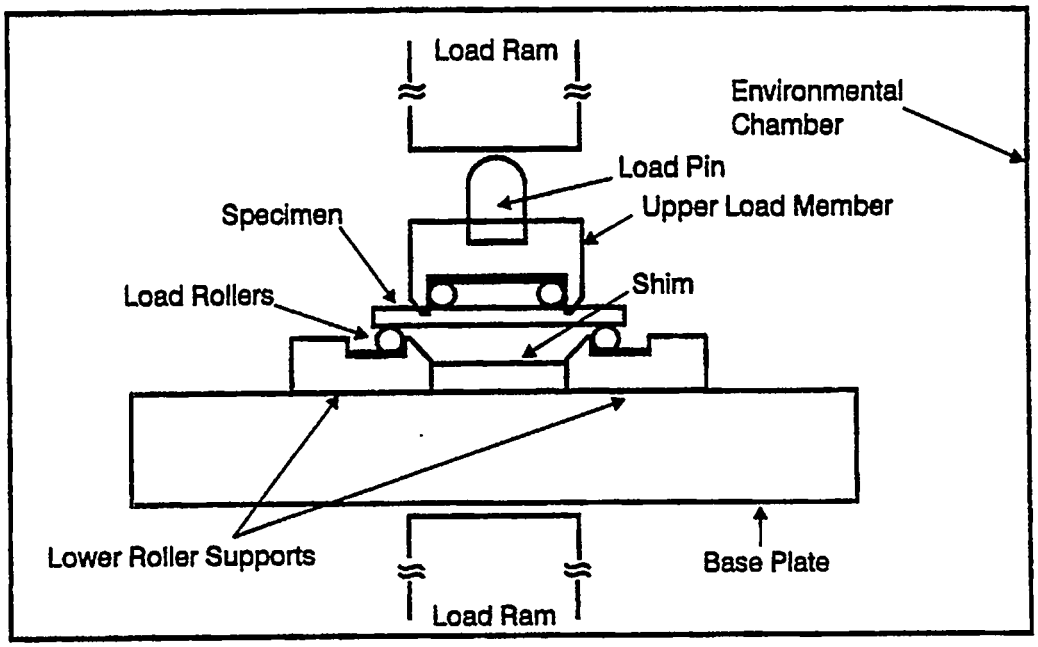

Figure 11. Sketch of Flexure Fixture.

AIR HEATER MATERIALS

A 100-hour pilot-scale slagging combustion test of a prototype HITAF heat exchanger panel is planned for the present program. The test panel will be constructed of B1900, a castable nickel-based alloy, and will be covered with several types of refractory brick and monolithic refractories. Eleven possible refractory brick materials, three alumina-zirconia-silica (AZS), four chromia—alumina, and four alumina, were identified for use in the evaluation of the panel. UTRC provided an initial list of possible refractory brick materials, which was refined at the Energy & Environmental Research Center (EERC) after consulting with refractory vendors. The materials were chosen for their relatively high thermal conductivities since their corrosion resistances in combustion environments are not well known. Properties of the AZS materials are listed in Table 5.

Table 5. AZS Refractory Brick for Pilot-Scale Testing

Material Name: (Manufacturer):	ERMOLD (Corhart)	ERMOLD 300 (Corhart)	UNICORE 1 ER 1711 (Corhart)	ER 2161 RT (Corhart)
Composition, wt%				
SiO_2	18.5	18.5	12.2	15.0
Al_2O_3	49.5	49.5	45.5	26.8
ZrO_2	30.0	30.0	41.0	27.5
Na_2O	1.0	1.0	1.0	1.2
Cr_2O_3	0.0	0.0	0.0	27.0
Other	1.0	1.0	0.3	2.5
Thermal Conductivity,				
W/m K @1588 K	1.95	1.95	5.5	5.5
Btu in./hr ft^2 °F @2400°F	13.50	13.5		
Density (ASTM C20),				
g/cm^3	3.20	3.2		4.0
lb/ft^3	200.0	200		250
Porosity (ASTM C20), %	9.5	9.5	Low	Low
Cold Crushing Strength,				
MPa	50	50		343
psi	7,200	7,200		49,780
Price per Standard Brick, $	95	30—90	90	200

All of the AZS bricks are manufactured by Corhart Refractories Corporation and contain between 28 and 41 wt% ZrO_2. The thermal conductivities of the bricks increase with increasing ZrO_2 or Cr_2O_3 content. Of the four chromia-containing bricks, three are manufactured by Harbison-Walker, and one is manufactured by Carborundum (Table 6). The properties of the three alumina refractory brick materials are listed in Table 7.

Table 6. Chromia-Based Refractory Brick for Pilot-Scale Testing

Material Name: (Manufacturer):	Monofrax M K3 (Carborundum)	Ruby HD (Harbison-Walker)	Ruby SR (Harbison-Walker	Aurex 30SR WL-5167 (Harbison-Walker)
Composition, wt%				
SiO_2	1.6	0.8	1.9	1.9
Al_2O_3	58.6	87.0	83.6	63.1
Cr_2O_3	27.1	8.9	10.2	29.9
Fe_2O_3	5.9	0.2	0.2	0.1
MgO	6.1	0.3	0.1	0.2
Other	0.7	2.8 (TiO_2)	4.0	4.0 (ZrO_2)
Thermal Conductivity,				
W/m K @1588 K	3.6		20	
Btu in./hr ft^2 °F @2400°F	23.0			
Density (ASTM C20)				
g/cm^3	3.20	3.4	3.4	3.6
lb/ft^3	239.0	210	212	220
Porosity (ASTM C20), %	4.0	14.0	18.1	15.5
Cold Crushing Strength,				
MPa		121	88	
psi		17,500	12,700	12,990
Price per Standard Brick, $	178	20		44

Table 7. Alumina-Based Refractory Brick for Pilot-Scale Testing

Material Name: (Manufacturer):	Jargal M (Corhart)	Monofrax M (Carborundum)	Tufline 95 DM (Harbison-Walker)	Greentab SR (A. P. Green)
Composition, wt%				
SiO_2	0.5	0.8	2.0	12.7
Al_2O_3	95.0	94.5	94.2	86.0
Na_2O	4.0	3.8	0.0	0.2
Fe_2O_3	0.5	0.1	0.1	0.2
Other	0.0	0.8	3.7 (ZrO_2)	0.9 (P_2O_5)
Thermal Conductivity,				
W/m K @1588 K	7.0	5.1		
Btu in./hr ft^2 F @2400°F		35.0	23	23
Density (ASTM C20)				
g/cm^3	3.5	3.4	3.3	3.3
lb/ft^3		212.0	210.0	210.0
Porosity (ASTM C20), %		2.0	12.0	12.0
Cold Crushing Strength,				
MPa	200			
psi				
Price per Standard Brick, $	150	119		

PILOT-SCALE TESTING OF AIR HEATER ALLOY AND REFRACTORIES

Because of the need to reduce technical risks and adhere to schedules, the focus of the HITAF air heater materials has moved from advanced ceramics to alloys. Several possible alloy materials are being investigated, including nickel-based super alloys, such as B1900 for the radiant air heater, and wrought alloys, such as the Haynes 230 or Hastelloy X, for the convective air heater. A 100-hr corrosion test will be performed on the B1900 nickel-based alloy protected by several different refractory materials. The tests will be performed, at simulated HITAF conditions, in a modified pulverized coal pilot-plant test combustor at the EERC. An isometric drawing of the Combustion Test Facility (CTF) and operating conditions were included in the last quarterly report. For combustion testing of bituminous coals, such as Illinois No. 6, the furnace is fired at a rate sufficient to maintain a furnace exit-gas temperature of 2200°F (1204°C), usually 650,000 Btu/hr, with excess air maintained near 20%.

An initial alloy test panel design for the radiant section of the CTF was reviewed and modified and is illustrated in Figure 12. The panel will be covered with 5 refractory bricks, selected from Tables 5, 6, and 7 (shown in previous sections of this report), and two types of castable refractories, an alumina-based and a SiC-based refractory.

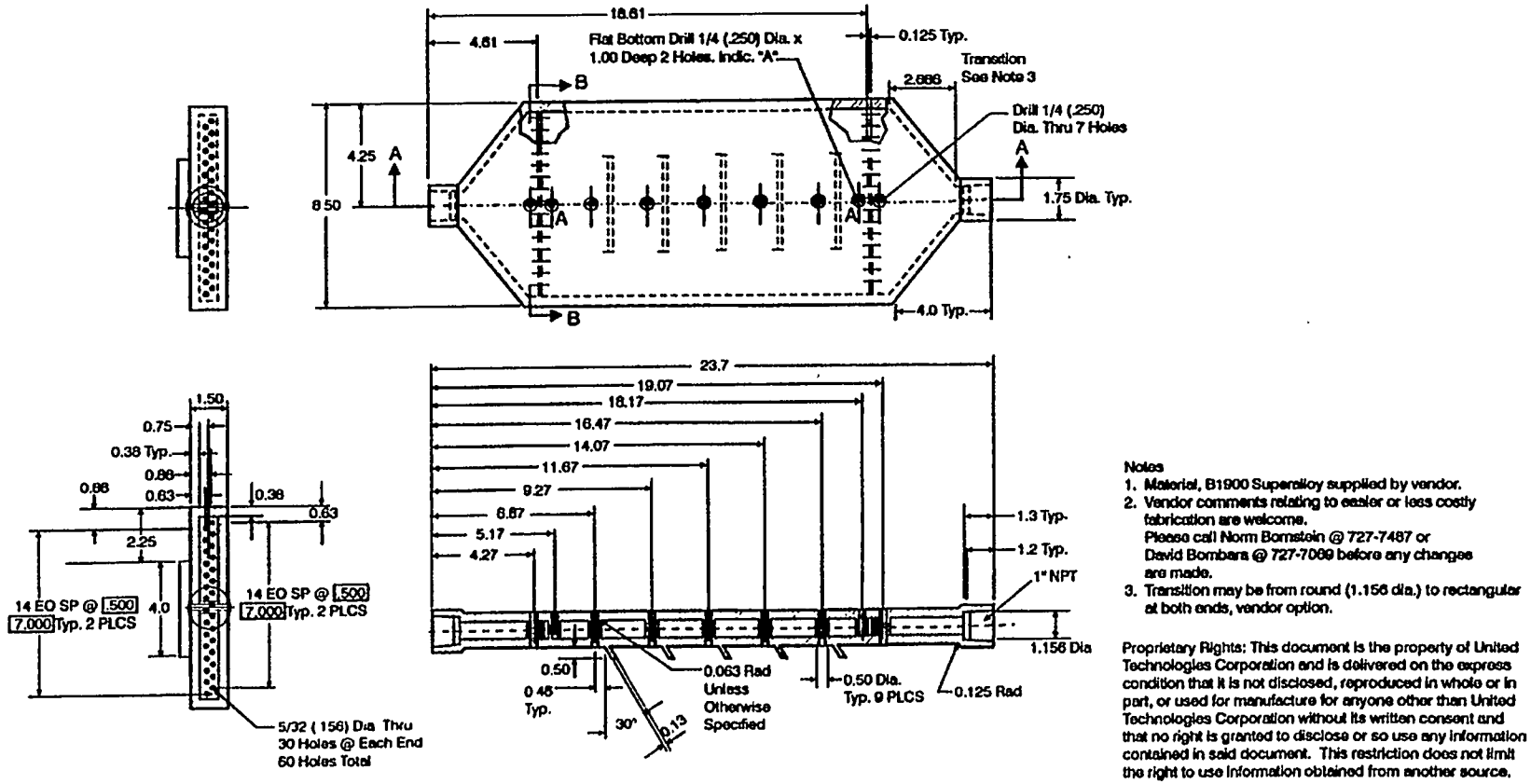

Notes
1. Material, B1900 Superalloy supplied by vendor.
2. Vendor comments relating to easier or less costly fabrication are welcome.
   Please call Norm Bornstein @ 727-7487 or
   David Bombara @ 727-7089 before any changes are made.
3. Transition may be from round (1.156 dia.) to rectangular at both ends, vendor option.

Figure 12. Top and Cross-Sectional View of the UTRC Alloy Test Panel Design (Units are Represented in Inches).

TEST PANEL DESIGN

The configurations for the alloy test panel and the test coupons have ben finalized. The original test panel design is reproduced in Figure 13. The test panel is essentially a thin box, approximately one inch wide. The design allows for thermocouple passageways for temperature measurements within the candidate ceramic bricks and in the cavity of the heat exchanger. Air enters the test panel through a 1 in. schedule 40 pipe and exits through a 2 in. schedule 40 pipe. The surfaces and pipes not protected by the candidate ceramics are protected from the furnace slag by a castable refractory. Lastly, a distribution plate located just above gas inlet insures proper gas flow through the box.

The design of the test panel is not representative of the actual design proposed for Combustion 2000. The test panel is designed to explore and determine the relative resistance of the candidate ceramics with respect to the molten slag, obtain experimental data for verification of thermal conductivities and heat transfer coefficients, and compatibility of metallic and ceramic materials.

After careful review of the test panel, the casting vendors expressed great reluctance. The areas of concern were (1) overall lengths, and (2) required tooling to produce an acceptable distribution plate. The final configuration, which is anticipated to be delivered to UTRC in the first week of March is shown in Figure 12.

The original length of the test panel, 29 1/2 inches, shown in Figure 13, coincides exactly with the ports in the EERC furnace. In the new design, the total length is about 24 inches. The UTRC machine shop will thread both ends. EERC will supply the threaded Haynes alloy pipe that connects the test panel to the air supply. (The current design includes the use of a compressible ceramic positioned between the metallic pipes and the castable ceramic that protects the pipes from the furnace environment. The compressible ceramic will absorb the stresses associated with the differences in expansion between the metal and the ceramics.)

The process to produce the threads has not been determined. Practice material has been supplied to the UTRC machine shop. The shop is investigating the use of cemented carbide taps or EDM. A final decision will be made late in February. The UTRC machine shop will also drill the 9 thermo-couple holes. The machine shop will evaluate the use of cemented carbide drills or EDM to produce the desired holes.

The details for the design of the refractory bricks has been completed and the design is shown in Figure 14. In the actual test, the bricks are supported by the castable ceramic applied by EERC. The metallic wings position the bricks, and as heat passes through the bricks to the metallic structure, the distance between the wings will grow as the wings grow into the ceramic. At temperature, the upward surface of the wing will be in intimate contact with the ceramic. The generous chamfer should prevent binding of the wing and the brick in the event that the calculations are in error.

The 30 degree chamfer at the base of the brick is designed to allow the molten slag to run "down" the brick. Although it was initially planned to examine the relative "penetrating power" of the molten

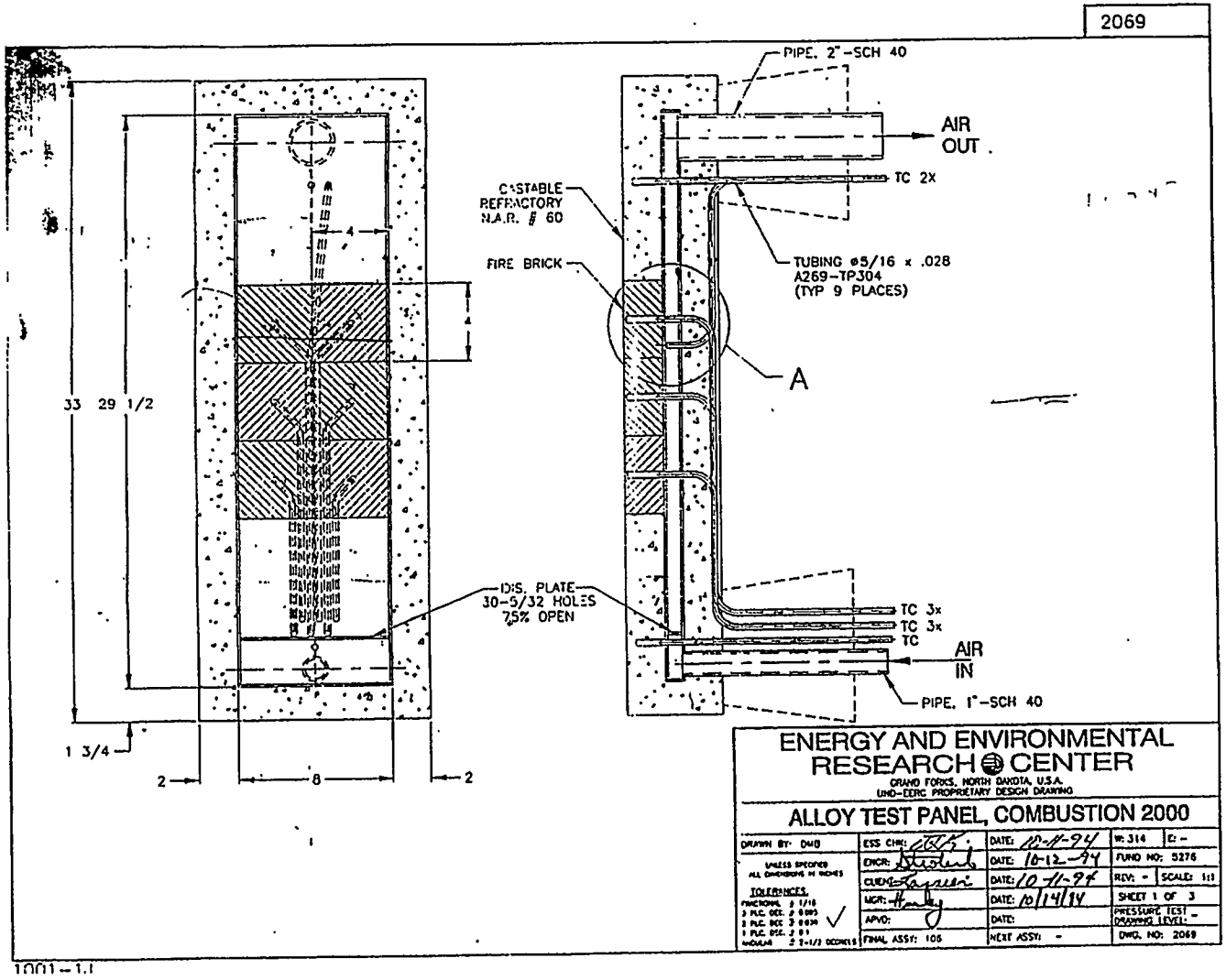

Figure 13. Alloy Test Panel, Combustion 2000.

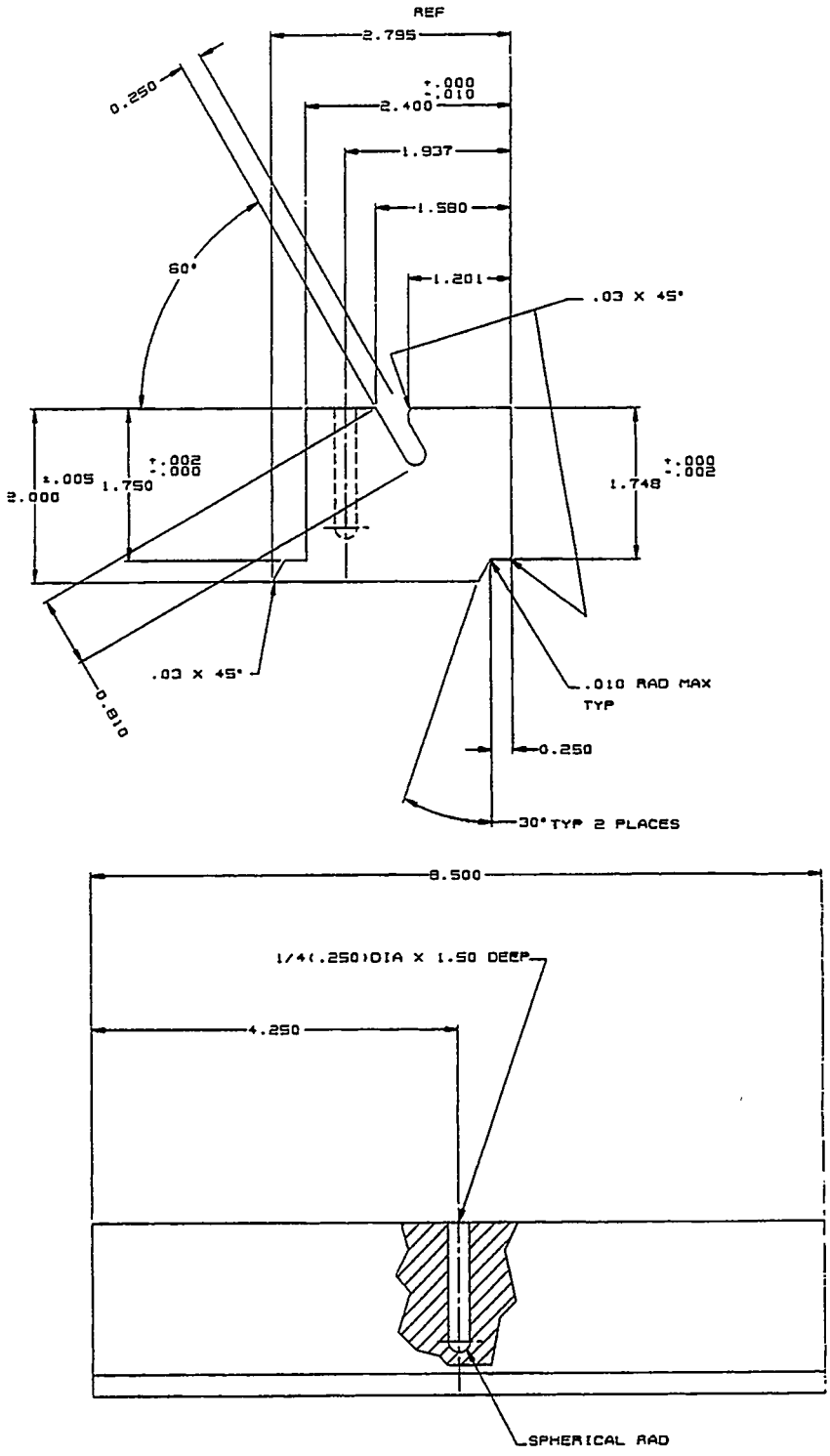

Figure 14. Design of Refractory Bricks.

slag at the interfaces where the brick comes together, the very high costs associated with separate machining of each brick overrode the uncertain knowledge gained by the experiment.

Lastly, the 1/4 in. dia hole will be filled with the thermocouples used to measure the temperature profile through the brick. The thermocouple well penetrates 3/4ths the depth of the brick.

Laboratory Tests

The configuration of the test specimens for laboratory evaluation of material compatibility has also been finalized. The details are shown in Figure 15. At room temperature the nickel base alloy comfortably fits into the cavity machined into the ceramic candidate brick. The cavity size is exactly the same for each of the candidate bricks. The dimensions of the metal are altered for each of the bricks such that at the test temperature the greater expansion of the metal brings the test pieces into intimate contact. The test schedule is shown below in Table 8.

Table 8. Laboratory Compatibility Test Program

Experimental Design Plan			
Ceramic Candidate	**Temperature °F**		
	1800	**2000**	**2200**
Jargal M Alumina Tufline 95DM Bricks	A A	AB AB	ABC
ER 1711 Chromia ER2161RT Bricks	A A	AB AB	ABC
MonoFrax K-3 AZS WL-5167 Bricks	A A	AB AB	ABC
Material designation: Superalloy "A" Pre-oxidized preoxidized "B" Aluminide coated superalloy "C"			

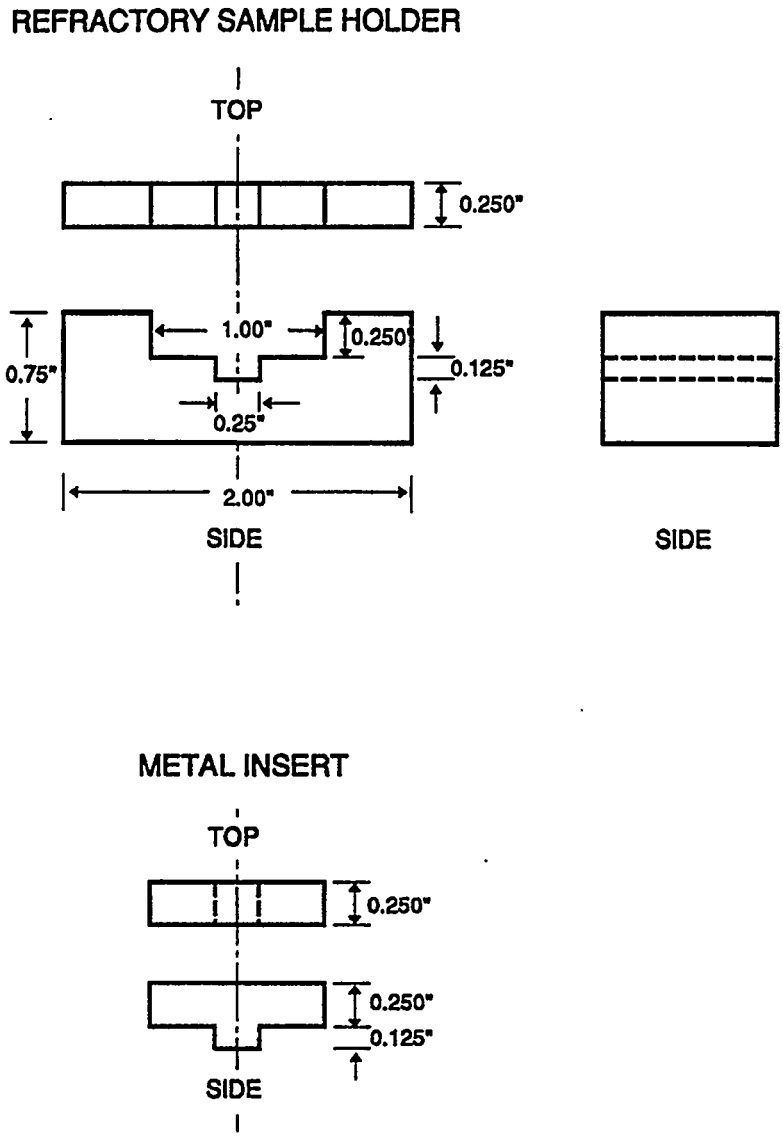

Figure 15. Refractory Sample Holder.